Mechanical properties of hydrogen-passivated silicon and silicon carbide nanoparticles

Laurent Pizzagalli, Jean Furstoss, Julien Godet, Julien Durinck, Sandrine Brochard

Mechanical properties of hydrogen-passivated silicon and silicon carbide nanoparticles

Laurent Pizzagalli, Jean Furstoss, Julien Godet, Julien Durinck, and Sandrine Brochard

Institut P′, CNRS UPR 3346, Université de Poitiers, SP2MI, Boulevard Marie et Pierre Curie, TSA 41123, 86073 Poitiers Cedex 9, France

E-mail: laurent.pizzagalli@univ-poitiers.fr

Abstract. Unlike the perfect models often used in numerical simulations, real nanoparticles are usually characterized by an oxidized or passivated surface, whose the effect on mechanical properties is not well known. In the present work we perform first principles molecular dynamics calculations to simulate the flat punch compression of small hydrogen passivated silicon and silicon carbide nanoparticles. They reveal that the nanoparticles yield at high strains and preferentially by amorphization. Small rotations are often observed before yielding. Our investigations suggest that these rotations are favored by the presence of the hydrogen passivated layer. Another consequence is a notable reduction of stiffness, due to the lower bending strength of Si/C-H bonds compared to the compression strength of the Si/C lattice. At last it is found that the amorphization of silicon carbide is facilitated by the presence of the hydrogen passivated layer.

Keywords: Nanoparticles; Mechanical properties; Silicon; Silicon carbide

Submitted to: *Modelling Simul. Mater. Sci. Eng.*

1. Introduction

Mechanical properties like strength, ductility, or toughness, depend on materials dimensions because they hinge on multiple mechanisms occurring at different scales [1, 2]. For instance, it is well documented that nanopillars become stronger when their dimensions are reduced up to the nanoscale [3]. The commonly agreed explanations are that usual bulk plasticity sources are hindered or not active due to the reduced dimensions, and that other plasticity mechanisms are triggered at higher stresses [4, 5]. It is also observed that the toughness and ductility of bulk brittle materials tend to largely increase when dimensions are reduced [6]. Below a certain size, all brittle materials are expected to plastically deform with no cracks [7, 8]. It is then not surprising that the mechanical properties of nanomaterials like nanowires, nanopillars, nanoparticles, can be strikingly different from bulk material.

Nanoparticles (NP) form an especially interesting class of systems for the investigations of mechanical properties. NP are in fact used in various contexts and in numerous applications, for which the knowledge of their mechanical properties is desirable [9]. For instance, NP can be reinforcement materials in bulk or coating composite materials. They can also be used as abrasives to perform chemical-mechanical polishing of thin films, or as additives in lubricants for tribology applications [9]. It is then important to achieve a good knowledge of their mechanical properties.

As mentioned above, one of the most spectacular characteristic of NP is their extremely high strength. Most of available data concern metallic FCC [10–19], and BCC [20–22] NP. Large values are also reported for other classes of materials, like for instance oxides [23–25] and carbon-based systems [26–29]. This suggests that the strength increase associated with size reduction is a general phenomenon in nanoparticles. Another interesting finding is the increase of toughness and ductility in brittle materials like Si and SiC as dimensions are reduced. This aspect is well documented for NP, in particular thanks to a large number of dedicated investigations [8, 30–38].

These outstanding NP mechanical properties are observed in both experiments and numerical simulations, with an overall consensus [39]. Yet theoretical models are usually characterized by perfect geometries with well defined shapes, edges and facets. This is at odds with real NP, which may exhibit rough surfaces, blunt shapes, and include internal structural defects. Another overlooked parameter is the presence at the NP surface of oxide or surfactants in experiments. In fact most metals or semiconductors surfaces are highly reactive, and the formation of a thin oxide layer is difficult to avoid. It is not clear whether the presence of an oxide surface layer has a significant influence on the mechanical properties. Wagner et al. report no strength differences between oxide-free and oxidized cubic Si NP [34]. This contrasts with another experiment showing a large strength increase for oxidized spherical Si NP [40]. Finally, using molecular dynamics simulations Zare Pakzad et al. show that the strength of Si nanowires is reduced in presence of an oxide layer [41].

The formation of a surface oxide layer can be prevented by using a surfactant to cover the surface and suppress reactivity. For instance hydrogen passivation is a simple way to saturate the surfaces of Si NP [42]. A legitimate and unresolved question is the influence of this hydrogen-passivation layer (HPL) on mechanical properties. On the one hand, it is reasonable to assume that an atomically thick HPL could be neglected, especially for NP with dimensions of several tens or hundreds of nm. On the other hand, the onset of plasticity is often associated with the heterogeneous nucleation of dislocations. And past investigations reveal that dislocation nucleation at silicon surfaces could be inhibited in presence of an HPL [43]. To gain more insights on the influence of HPL on mechanical properties we investigate in the present work the mechanical properties of small hydrogen passivated Si and SiC NP (1-2 nm). The uniaxial compression of these NP is simulated using first principles molecular dynamics. We find that amorphization is the main stress relaxation mechanism, and that it occurs at strains greater than 0.2. It is also shown that the HPL reduces the stiffness, favors the rotation of the NP, and also facilitates the initiation of amorphization.

2. Methods

First principles molecular dynamics compression simulations are performed using Car-Parrinello formalism [44], as implemented in the Quantum Espresso package [45]. All NP models are encompassed in supercells large enough to allow for at least 10 Å between periodic replicas. A 25 Ry plane wave cutoff

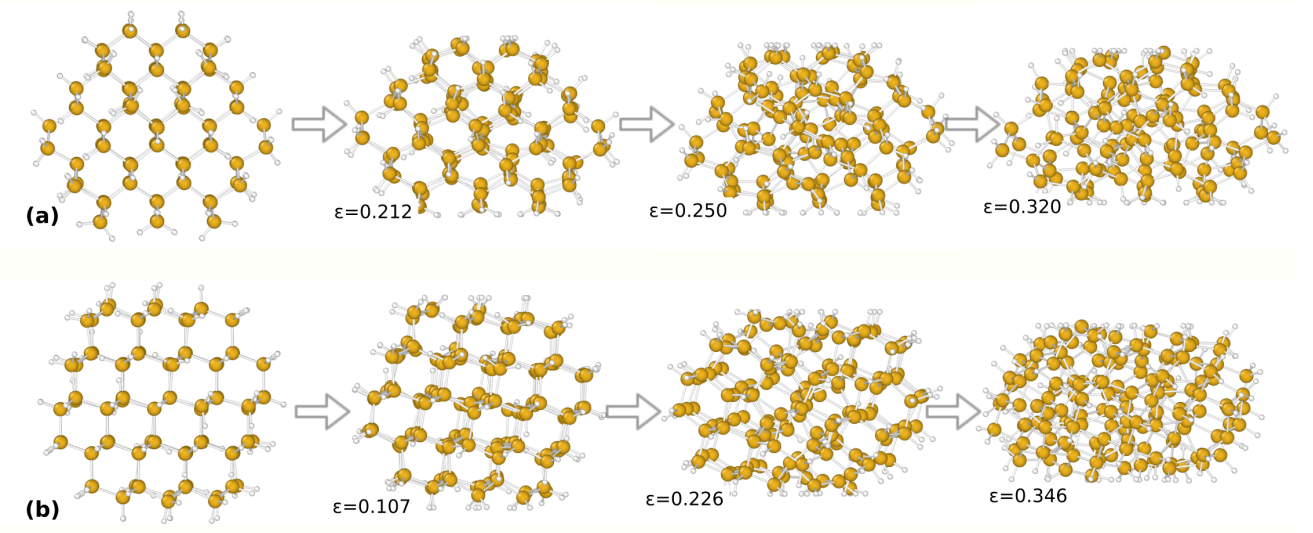

Figure 1. Configurations of Si NP models ($Si_{123}H_{100}$, ⟨001⟩ compression (a) and $Si_{148}H_{110}$, ⟨111⟩ compression (b)) at selected strain values. Leftmost structures represent the relaxed NP prior to compression. Silicon atoms are represented by golden spheres and hydrogen atoms by white spheres. Interatomic bonds are drawn according to distance criteria.

and a Γ-point sampling is used to compute the electronic structure. Exchange-correlation contributions are evaluated with the PBE functional [46], and the electron-ion interactions are modeled using ultrasoft pseudopotentials [47]. Stable dynamics are obtained with a timestep of 0.2 fs. We set the effective electron mass and the electron mass cutoff to 600 a.u. and 5 Ry, respectively [48]. Electronic and ionic degrees of freedom are controlled by Nose-Hoover thermostats, with an electronic kinetic energy target of 0.005 a.u. and an oscillation frequency of 90 THz for electrons, and a temperature target of 300 K and an oscillation frequency of 30 THz for the ions [49]. These parameters are appropriate for reliable dynamics [50, 51].

The compression of each NP is achieved according to the method described in Ref. [52]. Two planar classical repulsive force fields moving towards each other at a speed of 0.05 Å/ps are included in the simulation, yielding a compression speed of 0.1 Å/ps. All atoms with a height greater (lower) than the top (bottom) force field position feel a force proportional to the square of the height difference. A friction force is also added to these atoms, in order to prevent rotations about the compression axis [52]. The repulsion strength is set to 30 a.u., mimicking a very hard flat-punch indenter, and the friction strength is set to 500 a.u. [52]. At the start of each simulation, the force field positions are set so as to allow thermalization of the NP before compression.

We consider six NP models, two made of cubic silicon, and the other four made of cubic silicon carbide. Half of the NP are compressed along the ⟨001⟩ crystallographic orientation, and the other half along ⟨111⟩. These models exhibit cuboctahedron or truncated octahedron shapes. Note that they are similar to those used in a previous investigation [53]. All surfaces are passivated by hydrogen atoms. ⟨001⟩ oriented NP exhibits contact surfaces with dihydride Si/C atoms, and ⟨111⟩ oriented NP contact surfaces with monohydride Si/C atoms.

The variations of the potential energy and of the compression forces exerted by the planar repulsive force fields are monitored during the compression. The reference energy is calculated by computing the average of potential energy during a molecular dynamics simulations with no applied compression (thermalization). The strain is determined relatively to the positions of the planar repulsive force fields, with a reference corresponding to forces deviating from zero.

3. Results

The atomic positions evolution during compression for all NP are provided as Supplementary Materials files in the *xyz* format. Figure 1-(a) shows $Si_{123}H_{100}$ at different strains when compressed along the ⟨001⟩ orientation. Up to $\varepsilon \simeq 0.22$, no topological changes are observed and the corresponding compression force variation is approximately linear (Fig. 2, green line), suggesting that the deformation is elastic. The deformation is nonetheless not homogeneous, with the largest distortions occurring at the contact surfaces. In particular, we observe a significant increase of $\widehat{HSiH}$ angles for dihydride Si atoms (the initial value being about 107°), leading to Si-H bonds almost parallel to the contact surfaces. Energy and compression

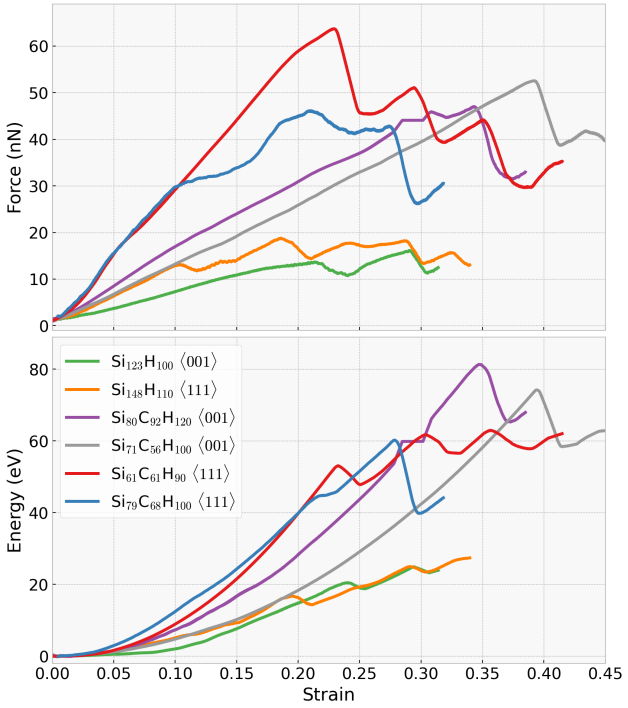

Figure 2. Compressive applied force (top graph) and energy (bottom graph) as a function of engineering strain for all NP models.

force drops occur when ε is $0.22 - 0.24$ although our analyses do not reveal specific structural changes. In a previous work we identified an elastic softening for the ⟨001⟩ compression of Si NP without HPL [53]. It is likely that the same phenomenon is happening here. Increasing further the strain leads to the progressive amorphization of the NP (Figure 1-(a)). The force and energy drops occurring at $\varepsilon \simeq 0.29$ (Fig. 2, green lines) correspond to a large structural relaxation of the disordered phase. The maximum contact force preceding the drop is 16.2 nN.

The second Si NP model is compressed along the ⟨111⟩ orientation (Figure 1-(b)). The compression force grows linearly only up $\varepsilon \simeq 0.10$, with a slope approximately twice the one for $Si_{123}H_{100}$ (Fig. 2, orange line). A similar stiffness difference is observed for non-passivated Si NP [53], which suggests that silicon elastic anisotropy is the main cause here, and not the HPL. A small force drop occurs at $\varepsilon \simeq 0.10$, corresponding to the rotation of the NP of about 10-15° around a ⟨110⟩ axis perpendicular to the compression orientation (Fig. 1-(b)). We emphasize that there is no plastic deformation when the NP rotates, although the contact force is noticeably decreased. Yield begins at $\varepsilon \simeq 0.19$ when the NP starts to amorphize from its center, with a maximum contact force of 18.8 nN. This mechanism is associated with small energy and force drops (Fig. 2, orange lines). When the strain is further increased the compression force fluctuates around a constant level while the energy grows as a whole, corresponding to the stress-assisted amorphization expanding over the NP. Structural analyses of the disordered phase in $Si_{123}H_{100}$ and $Si_{148}H_{110}$ reveal that the Si atoms coordination remains mostly 4-fold with a limited increase of 5-fold occurences, in agreement with previous works [54].

Figure 3 shows the four SiC NP at various stages of compression. We focus first on $Si_{80}C_{92}H_{120}$ compressed along ⟨001⟩ (Fig. 3-(a)). The most prominent feature of this case is the impressive strain range of the elastic regime. In fact, we find that the NP can be compressed up to $\varepsilon \simeq 0.34$, while preserving the initial crystalline structure. At this strain, the Si-H bonds at the contact surfaces are bent so as to have the $\widehat{HSiH}$ angles close to 180°, with surface Si/C/H atoms at the same height. Small ripples in the force curve for $\varepsilon < 0.34$ are associated with slight rotations of the NP (Fig. 2, purple line). At $\varepsilon \simeq 0.34$ and a contact force of 47.0 nN, we observe the initiation of amorphization (Fig. 3-(a)), followed by significant drops in both force and energy. A close behavior is obtained for $Si_{71}C_{56}H_{100}$ and the same compression orientation (Fig. 3-(b)). A linear variation of the compression force can be here observed up to $\varepsilon \simeq 0.39$. The SiC structure is markedly compressed, and the Si-H bonds at the surfaces are progressively flattened, like in the previous case. At larger strains, the NP becomes disordered, which decreases both the force and the energy (Fig. 2, grey lines). The maximum contact force associated with the onset of plasticity is 52.5 nN.

For ⟨111⟩ compressed SiC NP the predicted stress relaxation scenarios are slightly different. $Si_{61}C_{61}H_{90}$ can be compressed up to $\varepsilon \simeq 0.23$ with a linear force variation (Fig. 3-(c)), which corresponds to a maximum compressive force of 63 nN, the largest attainable value amongst all NP (Fig. 2, red line). Large force and energy drops are next observed when the strain increases. It corresponds to the rotation of the NP of about 20° around a ⟨110⟩ axis perpendicular to the compression orientation, which seemingly orientates the compression along a ⟨112⟩ direction. After a short reloading stage, a second relaxation stress event is observed at about $\varepsilon \simeq 0.30$ and a contact force of 51.0 nN. It consists of a collection of atomic displacements with small amplitudes, which appear to be mostly concentrated in the middle of the NP and lead to a shear seemingly localized in a {111} shuffle plane. Although shuffle set dislocations are known to be active during the plastic deformation at low temperature of covalent materials like Si [55–57] and SiC [58], it is not possible to claim that a dislocation nucleated and propagated as there is a lack of evidence and a significant amount of disorder. The

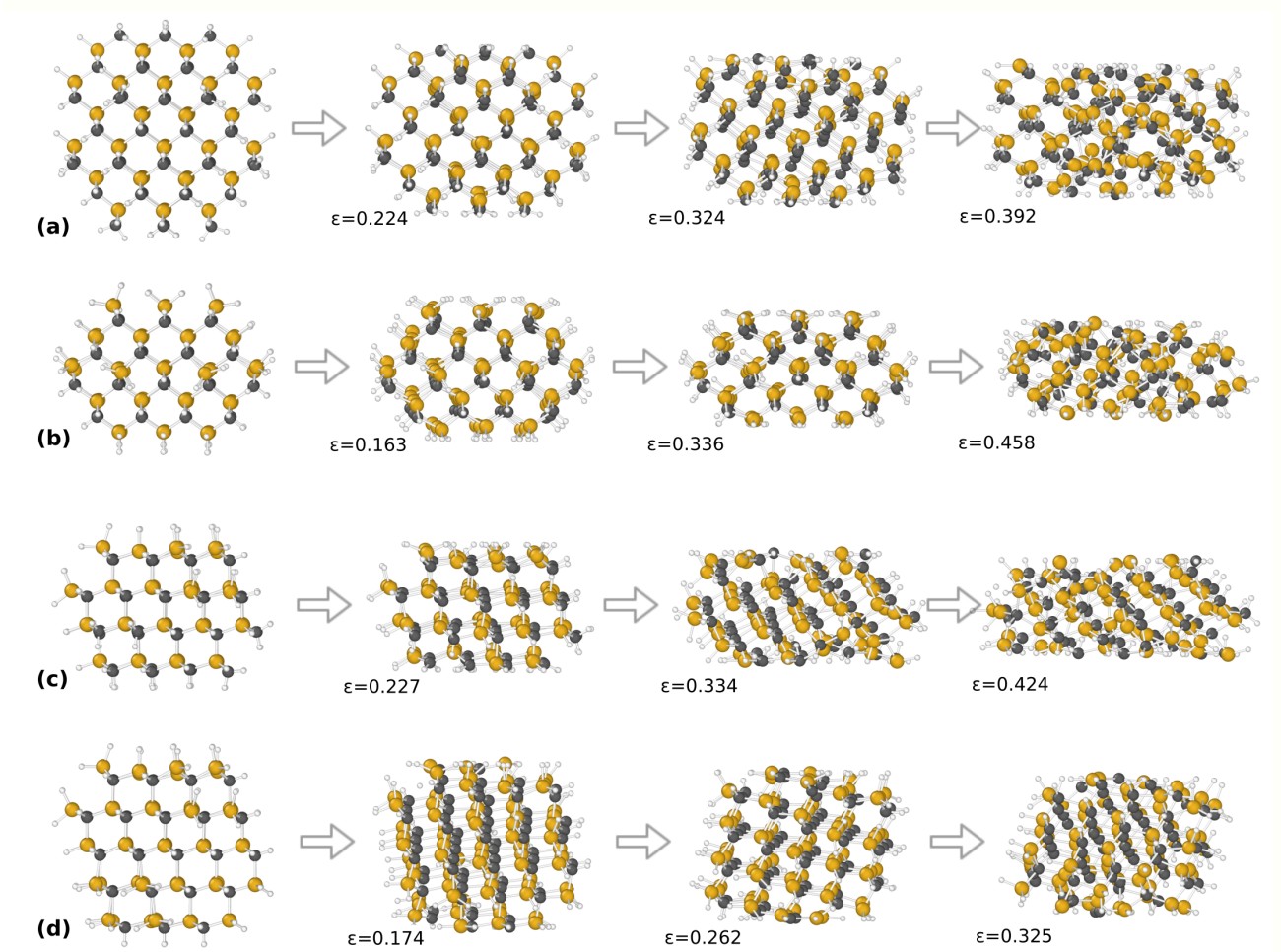

Figure 3. Configurations of SiC NP models ($Si_{80}C_{92}H_{120}$, ⟨001⟩ compression (a); $Si_{71}C_{56}H_{100}$, ⟨001⟩ compression (b); $Si_{61}C_{61}H_{90}$, ⟨111⟩ compression (c); and $Si_{79}C_{68}H_{100}$, ⟨111⟩ compression (d)) at selected strain values. Leftmost structures represent the relaxed NP prior to compression. Silicon atoms are represented by golden spheres, carbon atoms by black spheres, and hydrogen atoms by white spheres. Interatomic bonds are drawn according to distance criteria.

structure at the maximum strain overall retains its crystalline character (Fig. 3-(c)). At $\varepsilon \simeq 0.35$ a third stress relaxation mechanism is observed, leading to the partial amorphization of the NP (Fig. 3-(c)).

The last studied system is $Si_{79}C_{68}H_{100}$ compressed along ⟨111⟩. As for $Si_{123}H_{100}$, the linear variation domain of compression force is much smaller than the other NP, with a significant inflexion occurring at $\varepsilon \simeq 0.1$ (Fig. 2, blue line). Visual inspection reveals that it corresponds to the progressive rotation of the NP up to a strain of $\varepsilon \simeq 0.15$ (Fig. 3-(d)). The rotation appears to be similar than for $Si_{123}H_{100}$, with an amplitude of about 10-15° and a ⟨110⟩ rotation axis. This mechanism is nearly invisible on the energy curve (Fig. 2, blue line). A second force decrease and an energy inflexion occur at $\varepsilon \simeq 0.21$. They are associated with the progressive rotation of the NP, again of about 10-15°, but now with a ⟨112⟩ rotation axis perpendicular to the previous one (Fig. 3-(d)). As for other SiC NP, the Si/C-H bonds at contact surface are completely flattened at such a strain. Finally we observe large energy and force decreases starting at $\varepsilon \simeq 0.27$ (Fig. 2, blue lines). They are caused by the rupture of Si-C bonds at one of the contact surface, which allows for decreasing the NP height and relaxing the applied stress (Fig. 3-(d)). $\varepsilon \simeq 0.27$ is then the elastic limit at which plastic deformation starts, with a contact force of 42.7 nN.

In a nutshell, it is found that the first consequence of compressing the H-passivated Si and SiC NP is the progressive bending of Si-H and C-H bonds at the contact surfaces, which essentially occurs during the elastic regime. The primary drop in contact forces is often associated with a low amplitude rotation of the NP, especially for ⟨111⟩ compression cases. The next ones correspond to amorphization, which is the main stress relaxation mode. This result is in agreement with the literature. In fact amorphization is known to

be an efficient plasticity mechanism in high stress low temperature conditions [59, 60], as encountered here. It has also been observed or predicted in silicon [61, 62] and silicon carbide [63]. Other stress relaxation mechanisms are identified for $Si_{123}H_{100}$ compressed along $\langle 001 \rangle$, with an elastic softening preceding the amorphization, and for $Si_{61}C_{61}H_{90}$ compressed along $\langle 111 \rangle$ where some shear is observed. The NP strength, defined as the contact force at the beginning of plastic deformation, ranges from 16.2 to 18.8 nN for Si, and from 42.7 to 52.5 nN for SiC. These ranges are relatively narrow, which is reasonable given that our investigated systems have similar shapes and sizes.

4. Influence of HPL on mechanical properties

Table 1. Identified mechanisms during the compression of Si and SiC NP (Ref. [53]), and with a compressed HPL (present work): elastic softening (ES), amorphization (A), rotation (R), dislocation nucleation (D), and shear (S).

Case	Ref. [53]	With HPL
Si_{123} $\langle 001 \rangle$	ES $\rightarrow$ A	ES $\rightarrow$ A
Si_{148} $\langle 111 \rangle$	A	R $\rightarrow$ A
$Si_{80}C_{92}$ $\langle 001 \rangle$	R $\rightarrow$ A	R $\rightarrow$ A
$Si_{71}C_{56}$ $\langle 001 \rangle$	A	A
$Si_{61}C_{61}$ $\langle 111 \rangle$	D $\rightarrow$ A	R $\rightarrow$ S$\rightarrow$ A
$Si_{79}C_{68}$ $\langle 111 \rangle$	D $\rightarrow$ A	R $\rightarrow$ R $\rightarrow$ A

In this section, we discuss the influence of the HPL on the mechanical properties of NP. Some of us have recently investigated the mechanical properties of similar NP models and orientations using a similar setup, but without a compressed HPL [53]. It is then interesting to compare these results to the present ones in order to reveal its influence. Table 1 shows the identified mechanisms in both cases. Similar scenarios are obtained for $\langle 001 \rangle$ compressed NP. However, for the $\langle 111 \rangle$ orientation, the compressed HPL favors the rotation of the NP in all cases, which hinders the nucleation of dislocation at higher strains [53]. A possible cause is the different conformation of Si/C-H bonds at {111} and {001} surfaces. Those are monohydride bonds for the former, and dihydride bonds for the latter. Monohydride bonds are initially parallel to the compression axis and bend in random directions during compression, which induces a restoring force parallel to the contact surface thus favoring the rotation. Conversely the two Si/C-H bonds of a dihydride surface bend symmetrically, with a restoring force parallel to the compression axis. Another interesting point is the occurrence of elastic softening in both cases for Si_{123} compressed along

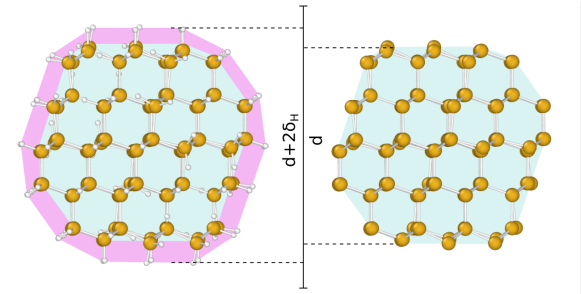

Figure 4. $Si_{148}H_{110}$ NP model, with (left) and without the hydrogen atoms (right). The cyan area shows the space occupied by silicon atoms, while the pink area shows the extra space associated with hydrogen atoms. The height of the NP is $d+2\delta_H$, with d the height of the uncovered NP and $2\delta_H$ the extra height due to the H atoms.

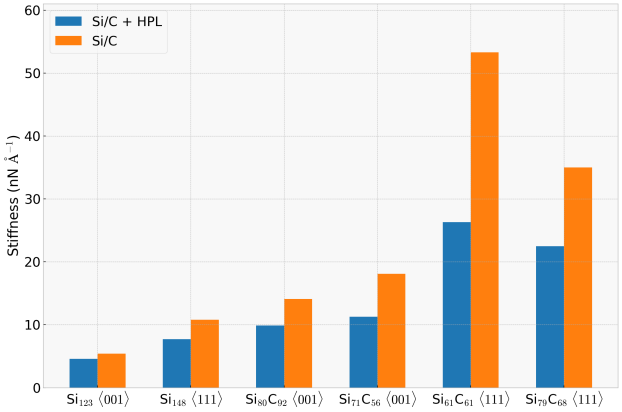

Figure 5. Influence of the HPL on the stiffness (nN $Å^{-1}$) for all investigated systems. The blue bars refer to the H-covered NP (present work), while the orange bars refer to NP with no compressed HPL (Ref. [53]).

$\langle 001 \rangle$, which suggests that the HPL has little influence on this mechanism.

We now try to achieve a quantitative assessment of the influence of HPL. Note that it is difficult to use normalized quantities such as the compression stress and the strain, since the initial dimensions of the NP with or without compressed HPL obviously differ (Fig. 4). In the remainder of this section, we then analyse the variations of the stiffness and of the height difference between the topmost and bottommost Si/C atoms, called d in the following (Fig. 4).

Figure 5 shows the stiffness values computed from the initial linear variation of the compression force in Fig. 2 associated with the elastic regime. We first note that the stiffness variations as a function of materials and orientations are qualitatively comparable to Young modulus variations. In fact, $E_{Si}^{001} = 129$ GPa $< E_{Si}^{111} =$ 189 GPa $< E_{SiC}^{001} =$345 GPa $< E_{SiC}^{111} =$541 GPa [64, 65]. Then we observe that there is a clear reduction due to the HPL in all cases. Using a core-shell model, it is straightforward to show that the inverse of the

stiffness of the H-passivated NP is the sum of the inverses of the stiffnesses of the HPL and of the Si/C core. With the reasonable assumption that the stiffness associated with Si-H and C-H bonds bending is lower than the stiffness for Si-Si and Si-C bonds compression, it explains why the stiffness of the H-passivated NP is reduced.

Next we examine the influence of HPL on the onset of plasticity. We compare d at which plastic deformation occurred, for a given NP with and with no compressed HPL. Si_{123} and $Si_{71}C_{56}$ are considered since these are the only two NP for which the plasticity mechanisms does not depend on the HPL (Tab. 1). For H-passivated Si_{123}, amorphization starts when the Si core height is $d = 10.3$ Å. This value is close to the one predicted for the amorphization of Si_{123} with no compressed HPL, i.e. 10.2 Å [53]. It suggests that the HPL influence is limited in that case. For H-passivated $Si_{71}C_{56}$ the amorphization occurs when the SiC core height is $d = 6.81$ Å. This is significantly larger than the value $d = 6.35$ Å at the onset of plasticity when no HPL is present. Therefore a higher compression level must be reached to initiate the amorphization of the SiC core with no compressed HPL. It suggests that the HPL has a substantial influence on the initiation of plasticity in that other case. A possible explanation is that the progressive bending of Si/C-H bonds in the HPL tends to lower the stability of the crystalline lattice in the vicinity of the concerned Si/C atoms, with respect to an amorphous phase.

5. Conclusions

In this work, first-principles molecular dynamics calculations are carried out to simulate the uniaxial compression of H-covered silicon and silicon carbide nanoparticles. It is found that the main stress relaxation mechanism is the amorphization of the NP at high strains, typically greater than 0.2. It is in most cases preceded by a low amplitude rotation of the NP associated with noticeable energy and compression force decreases. It is possible that these rotations could be dampened if the NP is not isolated and in contact with a liquid or other NP. We also observe one occurrence of elastic softening for the $\langle 001 \rangle$ compression of a Si NP, and a shear event for a SiC NP compressed along $\langle 111 \rangle$. The comparison of these results with a previous investigation [53] reveals that the presence of the HPL tends to favor the rotation of the NP during compression, especially for $\langle 111 \rangle$ oriented NP which exhibit monohydride contact surfaces. The presence of HPL also markedly decreases the stiffness, because it is easier to bend Si/C-H bonds in the HPL than to compress the Si or SiC lattice. Finally, the analysis of the two cases where similar mechanisms are observed with and without HPL, reveals that amorphization is facilitated by the presence of the HPL for a SiC NP.

The main limitation of this work is the limited set of investigated systems and their sizes. This is the price to pay for first-principles molecular dynamics calculations, which remain mandatory given the low reliability of interatomic potentials for describing nanoparticles or highly strained materials [66]. This issue could be circumvented in the future by designing appropriate machine learning potentials. Until then, it is always possible to speculate on the validity of our results for larger NP sizes. Regarding stiffness, the influence of HPL is expected to diminish as the NP size increases. However, the situation might be drastically different for plastic deformation, since its onset is expected to keep a local character. In that case, it is possible that the local weakening of the Si/SiC crystalline structure in the vicinity of the HPL could continue to play an important role even for much larger NP. Further investigations will be welcome to confirm or refute our predictions.

Acknowledgments

Computer time for this study was provided by the MCIA (Mésocentre de Calcul Intensif Aquitain). This work pertains to the French Government program "Investissements d'Avenir" (EUR INTREE, reference ANR-18-EURE-0010, and LABEX INTERACTIFS, reference ANR-11-LABX-0017-01).

References

[1] Lépinoux J, Mazière D, Pontikis V and Saada G (eds) 2000 *Multiscale phenomena in plasticity* NATO science series (Dordrecht [u.a.]: Kluwer) ISBN 0792362527 published in cooperation with NATO Scientific Affairs Division

[2] Kubin L 2013 *Dislocations, mesoscale simulations and plastic flow* Oxford Series on Materials Modelling (London: Oxford University Press)

[3] Uchic M D, Dimiduk D M, Florando J N and Nix W D 2004 *Science* **305** 986

[4] Uchic M D, Shade P A and Dimiduk D M 2009 *Annu. Rev. Mater. Res.* **39** 361–386

[5] Kraft O, Gruber P A, Mönig R and Weygand D 2010 *Annu. Rev. Mater. Res.* **40** 293–317

[6] Gerberich W W, Michler J, Mook W M, Ghisleni R, Östlund F, Stauffer D D and Ballarini R 2009 *J. Mater. Res.* **24** 898

[7] Kendall K 1978 *Nature* **272** 710

[8] Gerberich W W, Stauffer D D, Beaber A R and Tymiak N I 2012 *J. Mater. Res.* **27**(03) 552–561

[9] Guo D, Xie G and Luo J 2014 *J. Phys. D: Appl. Phys.* **47** 013001

[10] Mordehai D, Lee S W, Backes B, Srolovitz D J, Nix W D and Rabkin E 2011 *Acta Mater.* **59** 5202 – 5215

[11] Maaß R, Meza L, Gan B, Tin S and Greer J 2012 *Small* **8** 1869–1875

[12] Bian J J and Wang G F 2013 *J. Comput. Theor. Nanosci.* **10** 2299–2303

[13] Amodeo J, Begau C and Bitzek E 2014 *Mater. Res. Lett.* **2** 140–145

[14] Bel Haj Salah S, Gerard C and Pizzagalli L 2017 *Comput. Mat. Sci.* **129** 273–278

[15] Sharma A, Hickman J, Gazit N, Rabkin E and Mishin Y 2018 *Nat. Commun.* **9** 4102

[16] Kiani M T, Wang Y, Bertin N, Cai W and Gu X W 2019 *Nanoletters* **19** 255–260

[17] Zimmerman J, Bisht A, Mishin Y and Rabkin E 2021 *J. Mater. Sci.* **56** 18300–18312

[18] Griesbach C, Jeon S J, Rojas D F, Ponga M, Yazdi S, Pathak S, Mara N, Thomas E L and Thevamaran R 2021 *Acta Mater.* **214** 117020

[19] Pizzagalli L, Durinck J, Brochard S and Godet J 2024 *Scr. Mater.* **241** 115863

[20] Han W Z, Huang L, Ogata S, Kimizuka H, Yang Z C, Weinberger C, Li Q J, Liu B Y, Zhang X X, Li J, Ma E and Shan Z W 2015 *Adv. Mater.* **27** 3385–3390

[21] Bian J J, Yang L, Niu X R and Wang G F 2018 *Philos. Mag.* **98** 1848–1864

[22] Sharma A, Kositski R, Kovalenko O, Mordehai D and Rabkin E 2020 *Acta Mater.* **198** 72–84

[23] Calvié E, Réthoré J, Joly-Pottuz L, Meille S, Chevalier J, Garnier V, Jorand Y, Esnouf C, Epicier T, Quirk J and Masenelli-Varlot K 2014 *Materials Letters* **119** 107 – 110

[24] Issa I, Amodeo J, Réthoré J, Joly-Pottuz L, Esnouf C, Morthomas J, Perez M, Chevalier J and Masenelli-Varlot K 2015 *Acta Materialia* **86** 295 – 304

[25] Issa H K, Taherizadeh A and Maleki A 2020 *Ceramics International* **46** 21647–21656

[26] Yang W, Mao S, Yang J, Shang T, Song H, Mabon J, Swiech W, Vance J R, Yue Z, Dillon S J, Xu H and Xu B 2016 *Scientific Reports* **6**

[27] Jenei I Z, Dassenoy F, Epicier T, Khajeh A, Martini A, Uy D, Ghaednia H and Gangopadhyay A 2018 *Nanotechnology* **29** 085703

[28] Pascazio L, Martin J W, Bowal K, Akroyd J and Kraft M 2020 *Combustion and Flame* **219** 45 – 56

[29] Vidable G G, Gonzalez R, Valencia F, Amigo N, Tramontina D and Bringa E 2022 *Diamond Relat. Mater.* **126** 109109

[30] Valentini P, Gerberich W W and Dumitrică T 2007 *Phys. Rev. Lett.* **99**(17) 175701

[31] Lockwood A J and Inkson B J 2009 *J. Phys. D: Appl. Phys.* **42** 035410

[32] Beaber A, Nowak J, Ugurlu O, Mook W, Girshick S, Ballarini R and Gerberich W 2011 *Philos. Mag.* **91** 1179–1189

[33] Hale L, Zhang D B, Zhou X, Zimmerman J, Moody N, Dumitrica T, Ballarini R and Gerberich W 2012 *Comput. Mat. Sci.* **54** 280 – 286

[34] Wagner A J, Hintsala E D, Kumar P, Gerberich W W and Mkhoyan K A 2015 *Acta Mater.* **100** 256 – 265

[35] Hintsala E, Wagner A, Gerberich W and Mkhoyan K 2016 *Scr. Mater.* **114** 51 – 55

[36] Kilymis D, Gérard C, Amodeo J, Waghmare U and Pizzagalli L 2018 *Acta Mater.* **158** 155–166

[37] Kilymis D, Gérard C and Pizzagalli L 2019 *Acta Mater.* **164** 560–567

[38] Kayang K W and Volkov A N 2021 *Appl. Phys. A* **127** 921

[39] Amodeo J and Pizzagalli L 2021 *C.R. Phys.* **22** 1–32

[40] Xu W, Yu J, Ding J, Guo Y, Deng L, Zhang L, Wan X, Zheng S, Wang Y and Shan Z 2024 *Adv. Funct. Materials* **24** 2404694

[41] Zare Pakzad S, Nasr Esfahani M and Alaca B E 2023 *Materials Today Communications* **34** 105002

[42] Kang Z, Liu Y and Lee S T 2011 *Nanoscale* **3**(3) 777–791

[43] Godet J, Brochard S, Pizzagalli L, Beauchamp P and Soler J M 2006 *Phys. Rev. B* **73** 092105

[44] Car R and Parrinello M 1985 *Phys. Rev. Lett.* **55** 2471

[45] Giannozzi P, Andreussi O, Brumme T, Bunau O, Nardelli M B, Calandra M, Car R, Cavazzoni C, Ceresoli D, Cococcioni M, Colonna N, Carnimeo I, Corso A D, de Gironcoli S, Delugas P, DiStasio R A, Ferretti A, Floris A, Fratesi G, Fugallo G, Gebauer R, Gerstmann U, Giustino F, Gorni T, Jia J, Kawamura M, Ko H Y, Kokalj A, Küçükbenli E, Lazzeri M, Marsili M, Marzari N, Mauri F, Nguyen N L, Nguyen H V, de-la Roza A O, Paulatto L, Poncé S, Rocca D, Sabatini R, Santra B, Schlipf M, Seitsonen A P, Smogunov A, Timrov I, Thonhauser T, Umari P, Vast N, Wu X and Baroni S 2017 *J. Phys.: Condens. Matter* **29** 465901

[46] Perdew J P, Burke K and Ernzerhof M 1996 *Phys. Rev. Lett.* **77** 3865–3868

[47] Vanderbilt D 1990 *Phys. Rev. B* **41** 7892–7895

[48] Tassone F, Mauri F and Car R 1994 *Phys. Rev. B* **50** 10561–10573

[49] Thijssen J M 2000 *Computational Physics* (Cambridge: Cambridge University Press)

[50] Pizzagalli L 2022 *Phys. Chem. Chem. Phys.* **24** 9449–9458

[51] Pizzagalli L 2022 *Diamond Relat. Mater.* **123** 108870

[52] Pizzagalli L 2020 *Phys. Rev. B* **102** 094102

[53] Pizzagalli L and Godet J 2023 *Phys. Rev. Lett.* **131** 236201

[54] Kilymis D, Gerard C and Pizzagalli L 2019 Mechanical properties of amorphous silicon nanoparticles *The Minerals, Metals & Materials Series* The Minerals, Metals & Materials Series (Springer Berlin Heidelberg) pp 1347–1354

[55] Pizzagalli L, Beauchamp P and Jónsson H 2008 *Philos. Mag.* **88** 91

[56] Rabier J, Pizzagalli L and Demenet J L 2010 Dislocations in silicon at high stress *Dislocation in solids* vol 16 ed Kubin L and Hirth J P (Elsevier) chap 93, p 47

[57] Merabet A, Texier M, Tromas C, Brochard S, Pizzagalli L, Thilly L, Rabier J, Talneau A, Vaillant Y M L, Thomas O and Godet J 2018 *Acta Mater.* **161** 54–60

[58] Pizzagalli L 2014 *Acta Mater.* **78** 236 – 244

[59] Idrissi H, Carrez P and Cordier P 2022 *Curr. Opinion in Sol. Sta. & Mat. Sci.* **26** 100976

[60] Li B, Li A, Zhao S and Meyers M 2022 *Mater. Sci. Eng. R: Reports* **149** 100673

[61] He Y, Zhong L, Fan F, Wang C, Zhu T and Mao S X 2016 *Nature Nanotechnology* **11** 866–871

[62] Han J, Xu S, Sun J, Fang L and Zhu H 2017 *RSC Adv.* **7** 1357–1362

[63] Szlufarska I, Kalia R K, Nakano A and Vashishta P 2005 *Phys. Rev. B* **71**

[64] Hall J J 1967 *Phys. Rev.* **161** 756

[65] Pizzagalli L 2021 *Philos. Mag. Lett.* **101** 242–252

[66] Godet J, Pizzagalli L, Brochard S and Beauchamp P 2003 *J. Phys.: Condens. Matter* **15** 6943